ELSEVIER ELSEVIER

Contents lists available at ScienceDirect

# Earth and Planetary Science Letters

journal homepage: www.elsevier.com/locate/epsl



# Aseismic ridge subduction focused late Cenozoic exhumation above the Peruvian flat slab



Sarah W.M. George <sup>a,\*</sup>, Nicholas D. Perez <sup>b</sup>, William Struble <sup>a</sup>, Magdalena Ellis Curry <sup>c</sup>, Brian K. Horton <sup>d</sup>

- <sup>a</sup> Department of Geosciences, University of Arizona, Tucson, AZ, 85721, USA
- b Department of Geology & Geophysics, Texas A&M University, 3115 TAMU, College Station, TX 77843-3115, USA
- <sup>c</sup> Department of Marine, Earth, and Atmospheric Sciences, North Carolina State University, Raleigh, NC, 27695, USA
- d Department of Geological Sciences and Institute for Geophysics, Jackson School of Geosciences, University of Texas at Austin, Austin, TX 78712, USA

#### ARTICLE INFO

# Article history: Received 15 February 2022 Received in revised form 13 July 2022 Accepted 26 July 2022 Available online 11 November 2022 Editor: R. Bendick

Keywords: flat slab ridge subduction Nazca Ridge Andes mountains exhumation arc cessation

#### ABSTRACT

Subduction of aseismic ridges and flat slab subduction are important processes that punctuate Cordilleran orogenesis and may enhance exhumation and rock uplift in the overriding plate. Distinguishing between the two drivers is often challenging, as many modern flat slabs spatially coincide with subducting buoyant ridges. The Peruvian flat slab is the largest region of active flat slab subduction on Earth, spanning over 1300 km of the subducting Nazca plate along the western margin of South America. The flat slab is associated with two seafloor ridges: the Nazca Ridge at the southern terminus and the fully subducted Inca Plateau in the north. These aseismic ridges are spatially confined with respect to the flat slab, allowing assessment of the relative roles of aseismic ridge interactions and flat slab subduction in driving upper plate exhumation. We present: (1) a regional compilation of geochronologic ages of Andean igneous rocks, which track the spatio-temporal evolution of Neogene magmatic arc cessation and hence slab flattening; (2) calculated geomorphic indices, which document landscape perturbations and climatic or lithologic changes, (3) a summary of erosion rates from river catchments on the western Andean slope, and; (4) a regional synthesis of thermochronologic ages that reflect the timing and magnitude of upper crustal cooling.

Thermochronometric cooling ages systematically track the progressive passage of the Nazca Ridge, suggesting that the buoyant ridge focused exhumation in the overriding plate. Geomorphic indices demonstrate enhanced topography and steeper channels closer to the position of the subducted ridge. The spatial progression of basement block uplifts in Peru also coincides with the timing of ridge passage. In hinterland regions, >2 km of exhumation occurred since ca. 15 Ma above the Peruvian flat slab. For individual locations within the orogen, active rock uplift declines after ridge passage, suggesting that increased coupling is not maintained across the entirety of the flat slab. We argue that above broad zones of flat slab subduction, focused areas of aseismic ridge subduction concentrate upper-plate exhumation and uplift. These observations may be relevant to other flat slab systems, which exhibit a broad zone of arc shutoff with corridors of focused exhumation.

© 2022 Elsevier B.V. All rights reserved.

#### 1. Introduction

Periods of flat slab subduction, when a subducting slab shallows to a near-horizontal orientation, are generally considered to drive punctuated shifts in magmatism and deformation along Cordilleran margins (e.g., Dickinson and Snyder, 1978; Jordan et al., 1983; Gutscher et al., 2000a, 2000b; Ramos and Folguera, 2009; Finzel et al., 2011; Horton, 2018). While modern flat slabs occupy ~10%

of Earth's subduction zones and are straightforward to identify with seismicity and tomography (e.g., Gutscher et al., 2000b; Hayes et al., 2018) our understanding of the kinematic response in the overriding plate remains limited. Although subducting ridges are not necessary to generate zones of flat slab subduction (Skinner and Clayton, 2013), many modern zones of flat slab subduction coincide with subducting oceanic ridges, which can also drive exhumation in the overriding plate (Wipf et al., 2008; Spikings and Simpson, 2014). This co-occurrence in modern subduction zones obscures the relative roles of aseismic ridge subduction versus flat slab subduction in concentrating upper-plate exhumation.

<sup>\*</sup> Corresponding author at: 1040 E. 4th St, Tucson, AZ, 85712, USA. E-mail address: sarahwmgeorge@gmail.com (S.W.M. George).

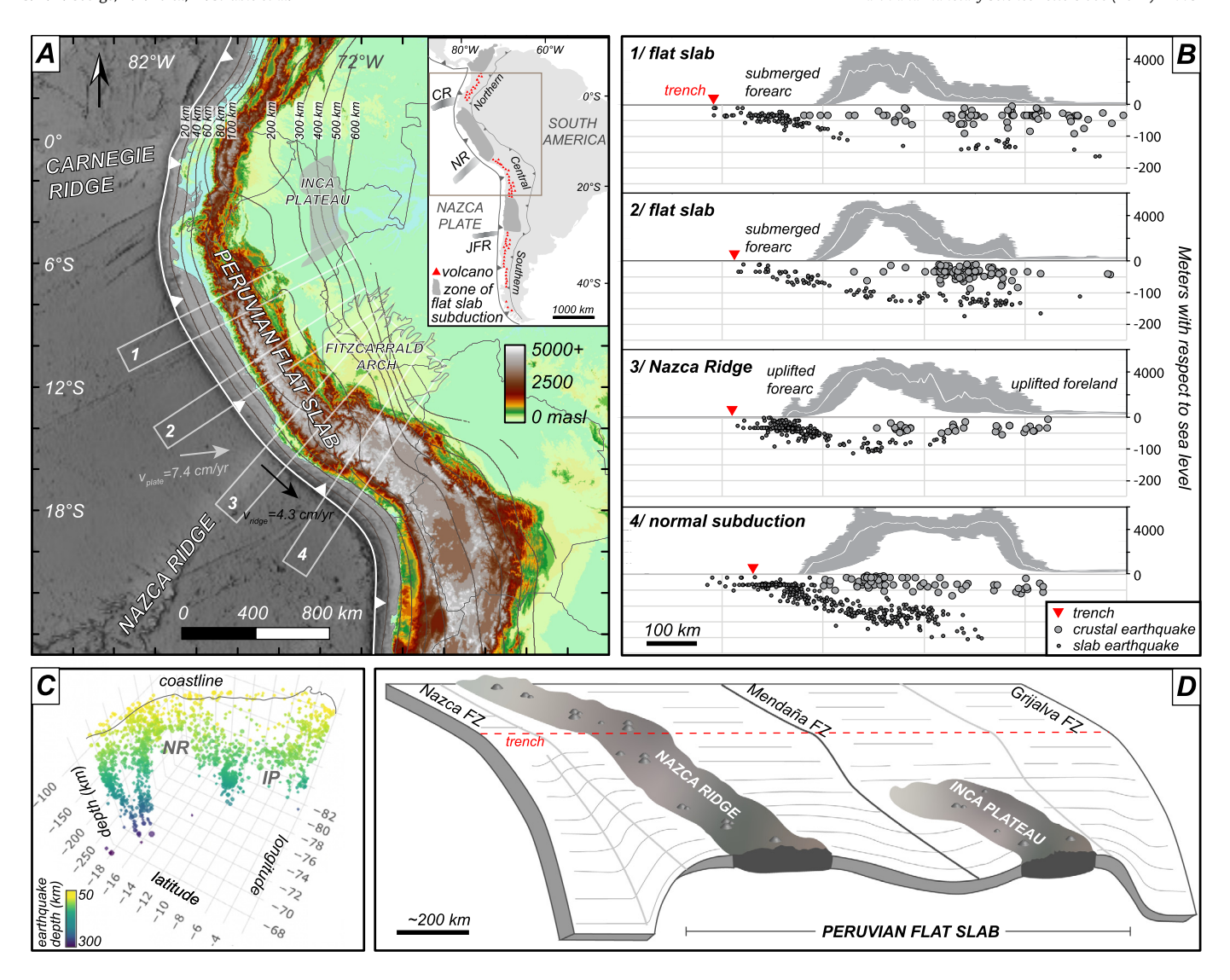


Fig. 1. (A) Digital elevation model of the Central and Northern Andes Mountains. Nazca slab Benioff contours, which define the top of the oceanic slab, are from Hayes et al. (2018). Trench parallel ridge velocity ( $v_{\text{ridge}}$ ) from Hampel (2002). Note the wide 100–200 km contour spacing that corresponds with the zone of flat slab subduction. Position of the subducted Inca plateau from Gutscher et al. (1999). Inset map after Horton (2018) with red triangles showing the Quaternary volcanic arc. CR = CARREDERION CR = CARREDER

Ancient zones of hypothesized flat slab subduction are identified from the inboard migration and subsequent shutoff of magmatic activity, propagation of deformation towards the foreland, often along high-angle, basement-involved structures, and fundamental changes in basin subsidence and sediment routing (e.g., Dickinson and Snyder, 1978; Jordan et al., 1983; Finzel et al., 2011). In North America, Laramide flat slab subduction, often linked to subduction of the Shatsky Plateau and Hess Rise conjugates, drove inboard migration of magmatic centers ~1000 km and caused a fundamental shift from dominantly thin-skinned, ramp-flat style structures to high-angle basement-cored uplifts (Dickinson and Snyder, 1978). Similar changes in deformation are documented in some active zones of flat slab subduction such as the Sierras Pampeanas of Argentina above the Pampean flat slab with the associated Juan Fernandez Ridge (e.g., Jordan et al., 1983), and the Alaskan flat slab above the thickened Yakutak microplate (Finzel et al., 2011). Other segments of flat slab subduction, such as in Mexico, appear to lack inboard basement-involved deformation (Manea et al., 2017).

However, the enhanced exhumation ascribed to flat slab subduction zones may instead be linked to interactions with subducting ridges on the seafloor (e.g., Rosenbaum and Mo, 2011; Spikings and Simpson, 2014; Morell, 2016). The Peruvian Andes contain the largest modern flat slab subduction segment, the Peruvian flat slab, spanning  $\sim$ 5–15°S (Fig. 1A) and occupying ca. 20% of the Andean subduction margin. The Peruvian flat slab corresponds with two buoyant features: the Nazca Ridge which is currently subducting near its southern terminus ( $\sim$ 15 $^{\circ}$ S), and the Inca Plateau, a plateau that has been fully subducted under South American continental lithosphere (~5°S; Gutscher et al., 2000b). Despite its spatial extent, the areas of active aseismic ridge subduction occupy only a small fraction of the spatial extent of the Peruvian flat slab (Fig. 1D). Tomography suggests direct contact between the top of the Nazca Ridge and overriding continental lithosphere (Bishop et al., 2017).

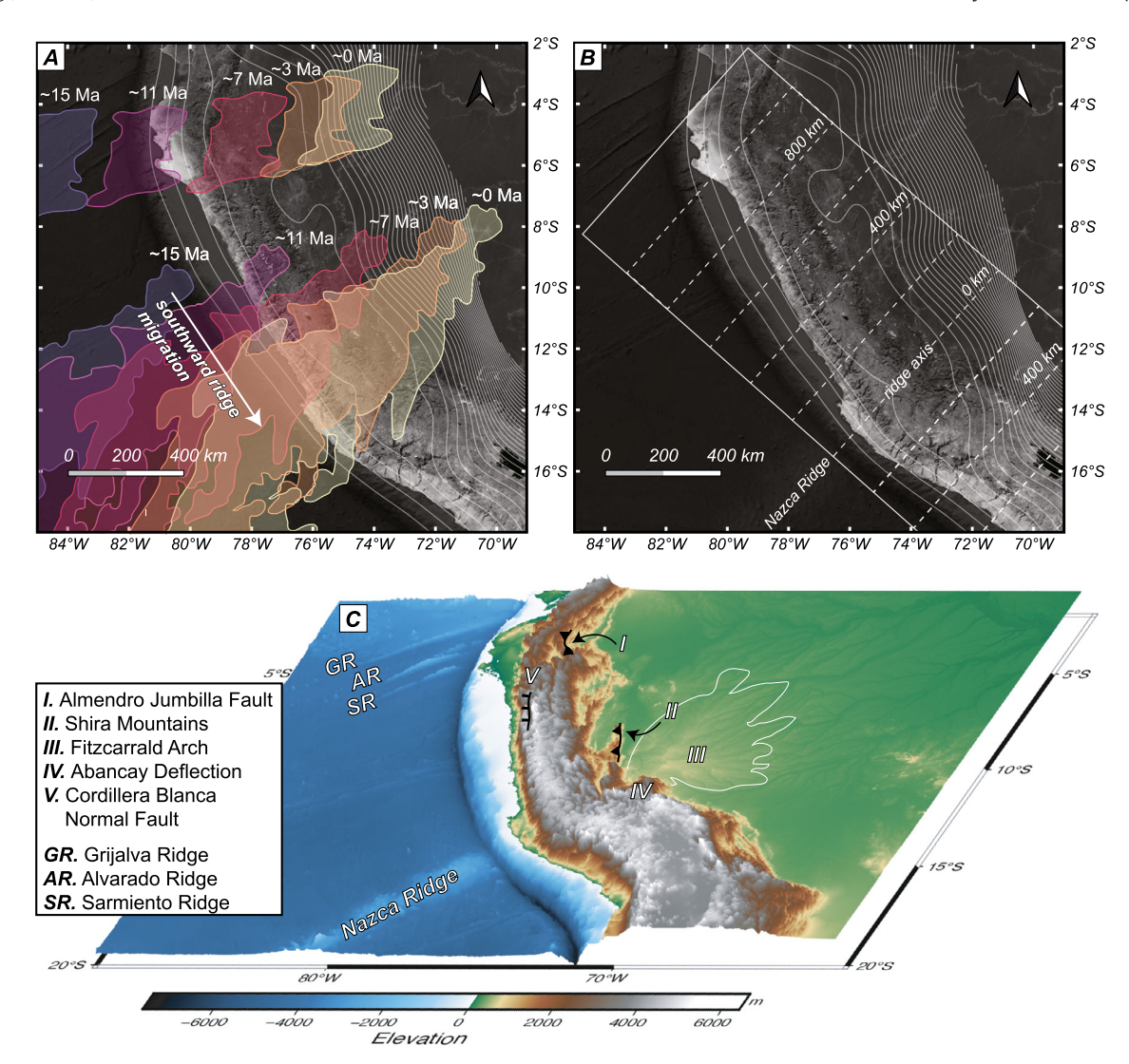


Fig. 2. (A) Migration history of the Nazca Ridge and Inca Plateau after Rosenbaum et al. (2005). (B) Distance from modern ridge axis, as used throughout the text and figures. Benioff contours are shown at 20 km intervals. (C) Key geomorphic features and sea floor ridges shown on an oblique digital elevation model.

The Peruvian flat slab has been the subject of geophysical studies defining the modern slab geometry and slab migration history (Barazangi and Isacks, 1976; Gutscher et al., 1999, 2000b; Rosenbaum et al., 2005; Bishop et al., 2017, 2018). These studies demonstrate that the Nazca Ridge intersected the trench in northern Peru in the middle Miocene and has swept progressively southward to its present location (Fig. 2A; Hampel, 2002; Rosenbaum et al., 2005). The relatively well-constrained geometry and migration history of the Nazca Ridge allow testing of the signals imparted on the rock record (Figs. 1 and 2). We present compiled datasets of high-temperature (U-Th-Pb, <sup>40</sup>Ar/<sup>39</sup>Ar, and K/Ar) geochronometers as indicators of arc cessation, low-temperature thermochronometers (apatite (U-Th)/He and fission-track) that record the timing of upper-crustal cooling, catchment-averaged erosion rates measured with cosmogenic nuclides to track transient landscape perturbations, and newly generated hypsometric profiles and normalized channel steepness of river profiles in the Western Cordillera to document landscape transience. We address the following questions:

(1) What were the spatio-temporal patterns and relative magnitudes of exhumation across the Andean region directly above the Peruvian flat slab? Specifically, was exhumation localized along discrete upper-crustal structures or broadly distributed

- across the landscape? Further, how did the rate and magnitude of exhumation above the subducting ridges (Nazca Ridge and Inca Plateau) compare to the remainder of the flat slab?
- (2) What mechanisms facilitate exhumation above zones of flat slab subduction, and do they operate uniformly across the flat slab, or are they spatially restricted to zones of enhanced mechanical coupling directly above subducting ridges and plateaus?

# 2. Geologic setting

## 2.1. The Nazca Ridge and the Inca Plateau

The northern and southern terminations of the Peruvian flat slab correspond to the proposed Inca Plateau and Nazca Ridge, respectively. Tomography and seismicity suggest that the slab is not laterally uniform in its subsurface geometry, and exhibits sags and spatially-restricted tears along-strike (Fig. 1; Gutscher et al., 1999; Antonijevic et al., 2015; Wagner and Okal, 2019). At the southern terminus is the  $\sim$ 200 km wide Nazca Ridge, a thickened portion of oceanic crust that intersected the trench at  $\sim$ 10°S between 15 Ma and 11.2 Ma and has been sweeping southward since to its current position at 15°S (Fig. 2A; Hampel, 2002; Rosenbaum et al., 2005). Geophysical surveying suggests that the ridge is  $\sim$ 17 km thick and

rises  $\sim$ 1.5 km from the seafloor, relative to the surrounding Nazca plate, which has an average 7 km oceanic crustal thickness (Hampel et al., 2004). The Nazca Ridge is considered to be a conjugate to the Tuamotu Plateau, which would have formed at the intersection between the East Pacific Rise and Easter-Salas Hotspot (Pilger, 1981; Gutscher et al., 1999; Hampel, 2002; Bishop et al., 2017).

The northern terminus of the flat slab region coincides with the proposed Inca Plateau, a fully subducted plateau that is thought to have reached the trench at ca. 13–10 Ma, and currently is located under the Santiago Basin of northernmost Peru (Figs. 1 and 2A; Gutscher et al., 1999, 2000b; Rosenbaum et al., 2005). The Marquesas Plateau in the Pacific Ocean is considered the most likely conjugate to the now subducted Inca Plateau (Gutscher et al., 1999; Rosenbaum et al., 2005).

## 2.2. Geologic overview

The Peruvian subduction zone has been active throughout most of the Paleozoic to present. Five tectonic domains characterize the flat slab region of Peru: the forearc, Western Cordillera, Eastern Cordillera, Subandean Zone, and foreland basin.

A relatively narrow series of low-relief forearc basins are preserved onshore and offshore along the coast of Peru. From north to south these include the Talara, Sechura-Salaverry, Pimentel, Trujillo, Lima, Huacho, Pisco, Paracas, Moquegua, and Mollendo Basins. These basins generally contain Cretaceous to Quaternary strata, typically deposited on Paleozoic metasedimentary rocks or Cretaceous arc-related rocks. The forearc basins have undergone significant subduction erosion since the middle Miocene (Clift et al., 2003; Hampel et al., 2004), yet differences in convergence velocities have been negligible since the Miocene (Maloney et al., 2013).

The Western Cordillera contains relatively high-elevation, high-relief peaks. Jurassic through Miocene arc rocks ranging from felsic to intermediate compositions dominate the Western Cordillera. In central-northern Peru, the Western Cordillera also hosts the Marañón fold-thrust belt, which was the locus of shortening throughout the Eocene (Mégard, 1984; Scherrenberg et al., 2016; Moreno et al., 2020). Since the late Miocene (~10 Ma) only restricted volcanic centers have been active in the Western Cordillera above the flat slab (e.g., Yanacocha and the Cordillera Blanca). The Western Cordillera also hosts the Cordillera Blanca normal fault and purported metamorphic core complex, interpreted to have formed during or after slab flattening (Fig. 2C; McNulty and Farber, 2002; Giovanni et al., 2010; Margirier et al., 2015).

The Eastern Cordillera is dominated by Paleozoic metamorphic and igneous rocks and Mesozoic sedimentary rocks, largely exposed along high-angle reverse faults and within the Marañón Anticline, a large-scale north plunging structure. At the northern terminus, the Eastern Cordillera is uplifted along a east-vergent high-angle fault, the Almendro Jumbilla Fault, and associated west-vergent back-thrusts (Fig. 2C; George et al., 2019; Moreno et al., 2020).

The Subandean Zone hosts the Miocene to modern thin-skinned fold-thrust belt, which deforms Paleozoic to modern metasedimentary and sedimentary rocks. Locally, deformation is accommodated on high-angle basement-involved structures (e.g., Shira Mountains, Cushabatay High, Contamana High, and Moa Divisor Range). Finally, the modern foreland basin consists of the Santiago, Huallaga, and Ene-Camisea Basins (wedge-top) and the Marañón, Acre, and Ucayali Basins (foredeep). East of the deformation front, the Fitzcarrald Arch forms a foreland region of higher elevation (ca. 600 masl) in eastern Peru and western Brazil (Fig. 2C). The Fitzcarrald Arch represents a long wavelength basement uplift that likely initiated in response to the Nazca Ridge (Fig. 2C; Espurt et al., 2007; Bishop et al., 2018). Late Cenozoic uplift of the Fitzcarrald arch has

strongly impacted Amazonian subsidence and partitioned the foreland basin system (Espurt et al., 2007). Flexural modeling suggests that flat slab subduction drove both (i) dynamic uplift in regions directly overlying the flat segment of the slab and (ii) dynamic subsidence in distal foreland regions east of the flat slab, possibly explaining anomalously thick (>1 km) sedimentary deposits located far from the deformation front (Eakin et al., 2014).

The work herein focuses on the mechanisms and crustal responses to initiation and establishment of the modern flat slab configuration with discrete margins defined by aseismic ridge subduction.

#### 3. Methods

Geochronologic ages (n = 1288 reported ages) from Oligocene to Quaternary igneous rocks from 2–18°S were compiled from the literature and the INGEMMET database and were confirmed using the original publications. The compilation was filtered to exclude sedimentary and metamorphic ages and the final dataset is available in the Supplemental Materials. The dataset is not filtered on magmatic type, as compositional data is unavailable, and thus the compilation could include some data unrelated to arc magmatism; however, the location of most datapoints is consistent with the Cenozoic arc axis.

Hypsometric profiles of large (>500 km<sup>2</sup>) watersheds draining the western flank of the Peruvian Andes were generated using the Global Multi-resolution Terrain Elevation Data 2010 7.5-arcsecond Digital Elevation Model (DEM) and the Hypsometric Curves Raster Terrain Analysis tool in QGIS. Catchment-averaged normalized channel steepness values for these west-draining river networks were computed in MATLAB with TopoToolbox (Schwanghart and Scherler, 2014; Supplemental Materials). Catchment-averaged normalized channel steepness (ksn) values exhibit complex relationships with uplift rate, and are impacted by lithology, climate, and tectonics (e.g., Kirby and Whipple, 2012). To generate accurate k<sub>sn</sub> maps, we employed topographic and geologic maps to define individual catchment boundaries and ensure that drainages analyzed were limited to bedrock channels. Significant Cenozoic volcanic materials in catchments could modulate channel slope. Cenozoic volcanic rocks in catchments are largely restricted to south of the Nazca Ridge (Fig. 4 and Supplemental Materials). Finally, we identified catchments potentially impacted by recent glaciation and removed channels that flow through glacial valleys, as application of k<sub>sn</sub> is limited to bedrock, fluvial drainage networks (see Supplemental Materials).

Additionally, we compiled erosion rates from <sup>10</sup>Be cosmogenic nuclide studies in west draining catchments of the Western Cordillera. We present results for larger catchments (>500 km²) to avoid local signals and to examine regional spatial variations in erosion rate. Specifically, we use erosion rates presented in the OCTOPUS database (Codilean et al., 2018) because these data have been reprocessed for consistent data treatment, allowing for comparisons among datasets from different studies. In well-mixed catchments, the average concentration of <sup>10</sup>Be in detrital quartz reflects the average erosion rate of a watershed (Codilean et al., 2018 and references therein), typically on timescales of 10³–10⁵ years. Unlike thermochronometric data, these rates are not dependent on the geothermal gradient, which may change during slab shallowing.

Thermochronometric ages from igneous and metamorphic rocks (apatite (U-Th)/He n = 218; apatite fission track n = 273) were compiled between 2–18°S (Supplemental Materials). Non-metamorphosed sedimentary rocks were excluded due to the prevalence of partially reset ages. We incorporated thermochronometric ages from a variety of methods with variable closure temperatures including apatite (U-Th)/He and apatite fission track, Apatite

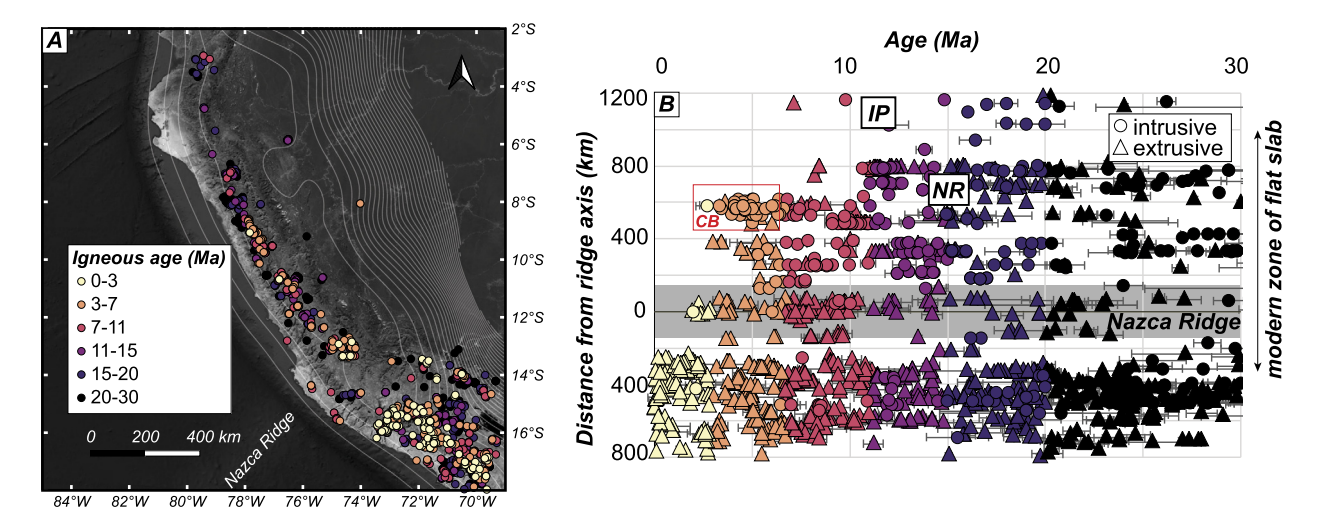
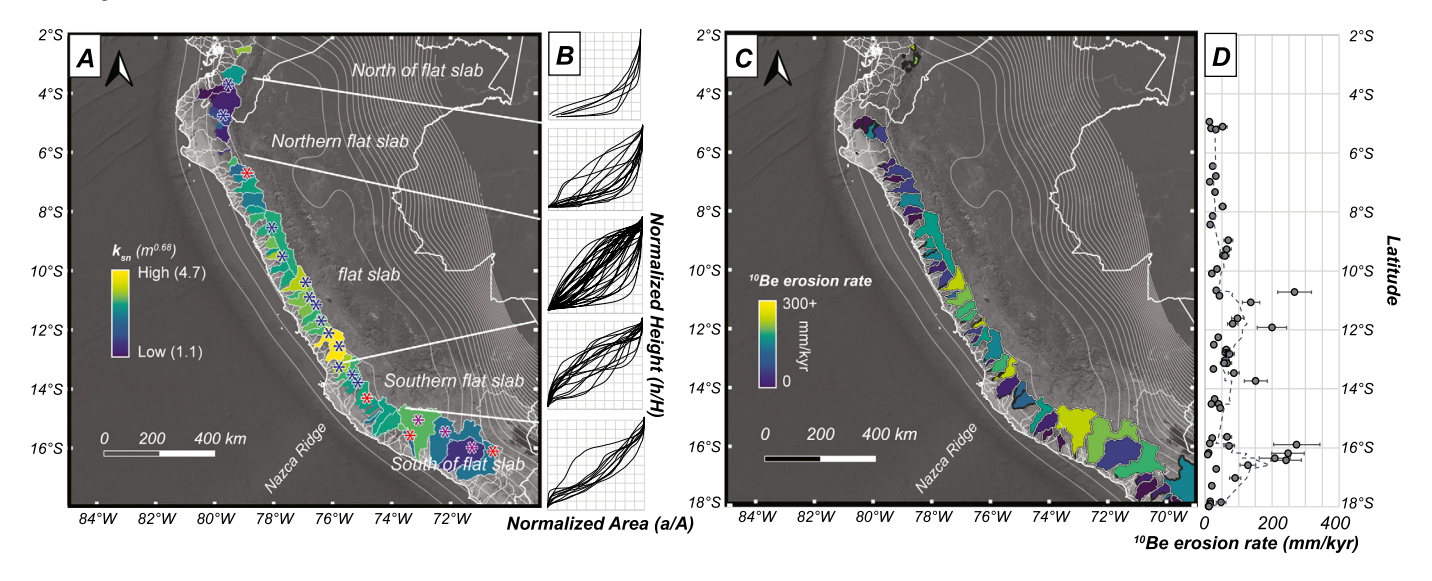


Fig. 3. (A) Map showing the distribution of dated magmatic deposits, colored by age. Benioff contours are shown at 20 km intervals. (B) Cross-plot of igneous ages (intrusive and extrusive) versus distance from the Nazca Ridge, highlighting the southward propagating arc shutoff starting in the late Miocene. Red box highlights magmatic centers associated with the Cordillera Blanca (CB) that remain active after the inferred timing of slab flattening. IP and NR show the timing and location where the Inca Plateau and Nazca Ridge intersected the trench. See text for additional details.



**Fig. 4.** (*A*) Map of catchment averaged normalized channel steepness  $(k_{sn})$  for west draining catchments >500 km² (using a calculated reference channel concavity; Supplemental Materials). Note that  $k_{sn}$  increases toward the current location of the Nazca Ridge. Blue asterisks indicate potential glaciation and red asterisks indicate significant Cenozoic volcanic rocks in headwaters. Purple asterisks indicate both. See Supplemental Materials for additional information. (*B*) Normalized hypsometric curves for catchments within the flat slab region versus to the north and south. Concave up profiles indicate fluvially incised landscapes, and concave down profiles correspond with catchments that are actively adjusting to a changing baselevel. (*C*) Map view of <sup>10</sup>Be erosion rates from the catchments in the Western Cordillera by latitude. Generally, erosion rates increase from north to south, toward the Nazca Ridge. (*D*) Cross-plot of <sup>10</sup>Be erosion rates from the catchments in the Western Cordillera by latitude with a moving average. See Supplemental Materials for data sources. Benioff contours are shown at 20 km intervals.

(U-Th)/He records cooling from  $\sim$ 50–110 °C, and the AFT system records cooling from  $\sim$ 90–140 °C, which collectively reflect exhumation from  $\sim$ 2–5 km, depending on the geothermal gradient (Ehlers and Farley, 2003; Ketcham et al., 2007). Specific closure temperatures depend on grain size, uranium concentration, and cooling rate (Ehlers and Farley, 2003). For fission track datasets, when both pooled and central ages are reported, we use the central age. For (U-Th)/He, we use weighted mean ages.

# 4. Results

#### 4.1. Southward propagation of arc shutoff

Magmatic ages in Peru show a latitudinal southward progression of arc shutoff, with no further arc magmatism after  $\sim$ 10 Ma at 5°S (Fig. 3). Arc magmatism in southern Peruvian localities shut off

around 4-2 Ma. This southward propagation of arc shutoff traces the reconstructed course of the Nazca Ridge through time (Fig. 2A). Rosenbaum et al. (2005) also considered the arc magmatic record of Peru and suggested that no convincing volcanic gaps existed before 4 Ma. New geochronologic constraints enable better constraints on the northern portion of the flat slab, where arc shutoff likely occurred earlier (ca. 10 Ma; Fig. 3). The Cordillera Blanca (CB of Fig. 3) exhibits younger ages than to the north or south. While these ages record the final magmatism during slab flattening (Coldwell et al., 2011) the youngest (<5 Ma) K/Ar and Ar/Ar ages likely represent cooling associated with large-displacement detachment faulting in the Cordillera Blanca, rather than magmatic crystallization. The eastward inboard sweep of magmatism remains poorly documented in Peru, potentially due to remote access in the Amazon Basin, though several Miocene-Pliocene igneous centers have been mapped and/or dated in the foreland (Fig. 3). Over-

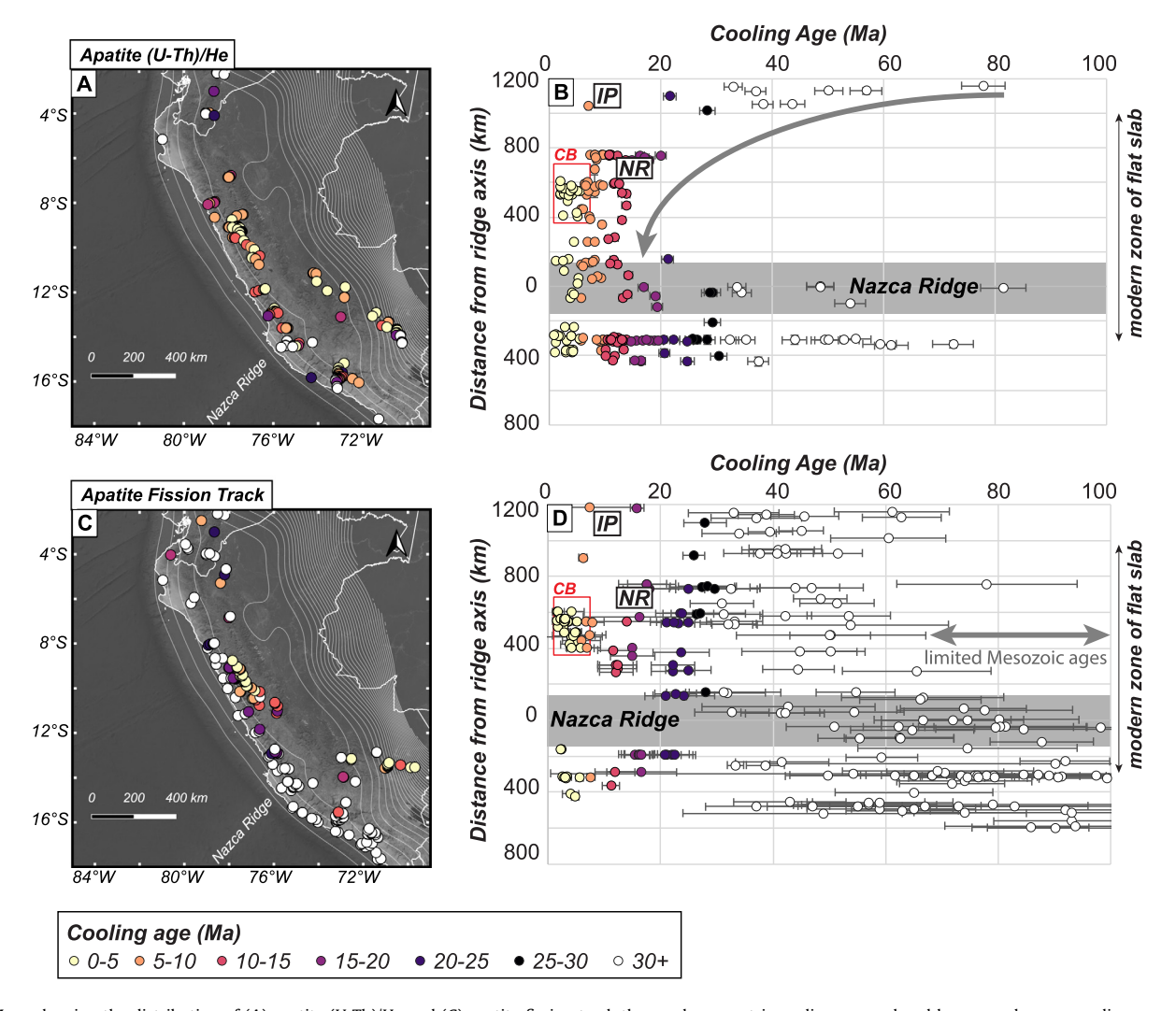


Fig. 5. Maps showing the distribution of (A) apatite (U-Th)/He and (C) apatite fission track thermochronometric cooling ages colored by age and corresponding cross-plots (B and D) of thermochronometric ages versus distance from the Nazca Ridge. Note the southward younging in the ages, and the step-function toward older ages at the terminus of the Nazca Ridge. The Cordillera Blanca (CB) shows young cooling ages, reflecting extensional exhumation on the Cordillera Blanca Normal Fault. IP and NR show the timing and location where the Inca Plateau and Nazca Ridge intersected the trench. Benioff contours are shown at 20 km intervals.

all, arc shutoff becomes systematically younger to the south, with shutoff around 10 Ma in the northern segment of the flat slab, and around 4–2 Ma in the southern portion near the Nazca Ridge. South of the Nazca Ridge, volcanism remains active.

## 4.2. Forearc drainage evolution

Geomorphic indices suggest transient and actively adjusting drainage systems above the Peruvian zone of flat slab subduction (Fig. 4). West-draining river networks within the flat slab (from 6–15°S) exhibit smaller catchments, steeper channels, and greater variation in hypsometric profiles than drainages to the north and south (Fig. 4). Concave down hypsometric profiles are most prevalent above the flat slab, and reflect high-elevation, low-relief landscapes that have not yet adjusted to base level. Elevated k<sub>sn</sub> values are nonuniform above the flat slab and indicate relatively steeper drainages north of the Nazca Ridge. Modern erosion rates from <sup>10</sup>Be cosmogenic nuclides show less pronounced spatial trends, though the northern drainages tend to have lower erosion rates than those in the south (Fig. 4C). At 16°S, erosion rates increase to >200 mm/kyr, well above the background value of  $\sim$ 60 mm/kyr along the rest of the Peruvian margin. The spike may reflect the leading edge of the Nazca Ridge, or may be controlled by the abundant, easily erodible volcanic rocks that fill the drainages south of the Nazca Ridge (Fig. 4D).

# 4.3. Magnitude and spatial extent of upper-crustal cooling

Thermochronometric ages in Peru exhibit strong spatial trends. Apatite (U-Th)/He analyses yield early to mid-Cenozoic cooling ages in the northernmost flat slab (~1200–1000 km north of the Nazca Ridge), and late Cenozoic cooling ages above the rest of the flat slab region (Fig. 5). A sharp, step-function shift occurs at the Nazca Ridge, with a highly varied distribution of ages spanning from the Late Cretaceous to late Cenozoic. A similar step-function is expressed in apatite fission track data, where mostly Cenozoic ages define regions above the flat slab, with a major shift toward broadly distributed ages (Mesozoic–Cenozoic) at the Nazca Ridge (Fig. 5D). The Cordillera Blanca (CB in Fig. 5) shows anomalously young cooling ages compared to surrounding areas, consistent with large-scale extensional exhumation since ~5.4 Ma (Giovanni et al., 2010; Margirier et al., 2016).

The spatial distribution of published thermochronometric constraints is not uniformly distributed across the study area. Despite this, two trends emerge: (1) the zone that the Nazca Ridge has interacted with has younger cooling ages than areas to the south or north, including zones that are within the modern flat

slab, as defined by the Benioff zone (Fig. 5), and (2) the youngest age peak generally is younger progressively southward toward the ridge (Fig. 6).

The compilation of thermochronometric data across Peru clarifies the spatial and temporal cooling patterns in the overriding plate. Apatite (U-Th)/He cooling ages tend to be younger than the timing of ridge passage (Fig. 5). For this to be true, there must have been  $\sim\!60^{\circ}\text{C}$  of cooling in areas where ridge passed. Apatite fission track ages mostly exhibit younger ages above the flat slab than to the south, but only the Cordillera Blanca has significant cooling ages that are younger than ridge subduction.

#### 5. Discussion

## 5.1. Controls on exhumation: flat slab or aseismic ridge subduction?

If flat slab subduction were the singular mechanism driving rock uplift in Peru, then signals associated with the flat slab should start earlier in the north but continue to be active across the entire flat slab. In contrast, if along-strike passage of the subducting ridge was the primary driver of exhumation, then patterns of thermochronologic ages and geomorphology would be expected to sweep southward and diminish after ridge passage. The regional thermochronologic and geomorphic datasets show strong spatial variability. Critically, we observe that the youngest apatite (U-Th)/He ages and highest k<sub>sn</sub> values are generally co-located and situated within the region through which the ridge has passed. Further, these cooling ages and geomorphic indices show clear spatial trends along-strike from north to south. In our discussion, we consider coupling to mean direct contact between the ridge and overriding plate, encompassing both forces related to shear along the interface as well as upward directed normal forces (ridge buoyancy). Above the modern location of the subducting Nazca Ridge, tomography shows removal of continental mantle lithosphere, and perhaps even thinning of the lower crust, requiring direct contact between the ridge and overriding crust (Bishop et al., 2017).

Thermochronometric ages decrease toward the south (Fig. 6), indicative of southward propagating exhumation that tracked the migration of the Nazca Ridge along the margin (this study; Wipf et al., 2008; Spikings and Simpson, 2014). While previous studies have emphasized increased coupling and forearc uplift (e.g., Hall et al., 2008; Wipf et al., 2008; Saillard et al., 2011) and foreland uplift (Fitzcarrald Arch; Espurt et al., 2007; Bishop et al., 2018) above the Nazca Ridge, this study also suggests increased hinterland exhumation centered directly above the subducting ridge (Fig. 7). Thermochronometric data reflect ridge-enhanced uppercrustal cooling up to  $\sim$ 550 km inboard from the trench (Fig. 7, similar to the extent of the flat slab region beneath Peru (e.g., Bishop et al., 2017). In addition to a comparable horizontal scale, the thermochronologic data provide first-order constraints on the amount of cooling attributable to ridge interactions. Apatite (U-Th)/He cooling ages not only post-date passage of the ridge, they also support 2 km of exhumation since the arrival of the Nazca Ridge at the trench. Young cooling ages, in the absence of surface breaking structures, have been documented in the Marañón foldthrust belt, and are attributed to underthrusting at depth (Scherrenberg et al., 2016).

Geomorphic indices, including  $k_{sn}$  and  $^{10}$ Be erosion rates, diminish northward away from the subducting Nazca Ridge (Fig. 4). Hypsometric curves show concave down drainage morphologies in the southern portion of the flat slab, suggesting that the drainages were recently perturbed and have not yet reached equilibrium profiles. Variability in these indices can be driven by a number of factors including rock uplift, drainage reorganization, climate, and lithology. The entire forearc region receives similar amounts of annual precipitation, and the study area is entirely located within the

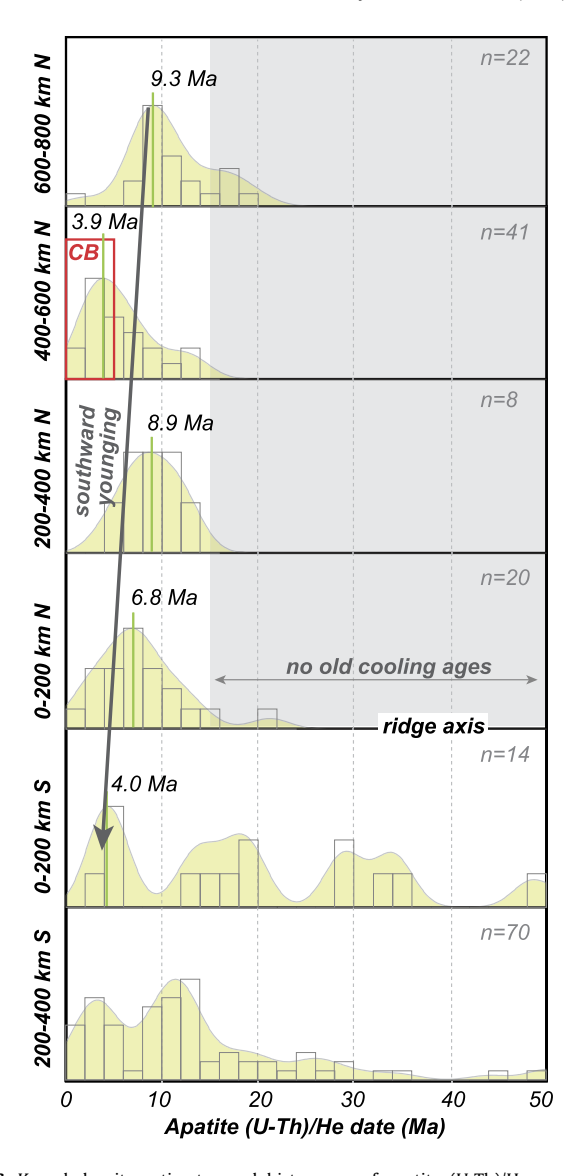


**Fig. 6.** Kernel density estimates and histograms of apatite (U-Th)/He ages across tectonomorphic domains binned by distance to the Nazca Ridge. Peak ages shown in green. Note the lack of cooling ages older than 15 Ma (the timing of ridge arrival) to the north of the Nazca Ridge. Young cooling ages in the Cordillera Blanca (CB) are related to extensional exhumation on the Cordillera Blanca Normal Fault (e.g., Margirier et al., 2015).

regional band of trade winds (Supplemental Materials); therefore, a strong climatic control on the along-strike variability is considered unlikely. Similarly, the magmatic arc materials of the Western Cordillera are relatively homogenous (Supplemental Materials). Although there is a change in lithology north of 8°S and south of 13.5°S, where sedimentary rocks are present in onshore forearc regions, we account for this change by limiting analysis to the inboard portions of the channels.

The spatial gradient in geomorphic indices is attributed to contrasts in rock uplift. Because the geomorphic indices are not uniform across the flat slab, and increase southward toward the Nazca Ridge, we suggest that rock uplift and associated drainage shifts were driven by ridge passage. Wipf et al. (2008) also emphasized drainage reorganization above the subducting Nazca Ridge, by showing that drainages above the ridge at altitudes <500 m do not take direct routes to the coast but are diverted to the northnorthwest and southeast and exhibit bimodal dispersal patterns. Similar observations have been made above the Cocos Ridge in

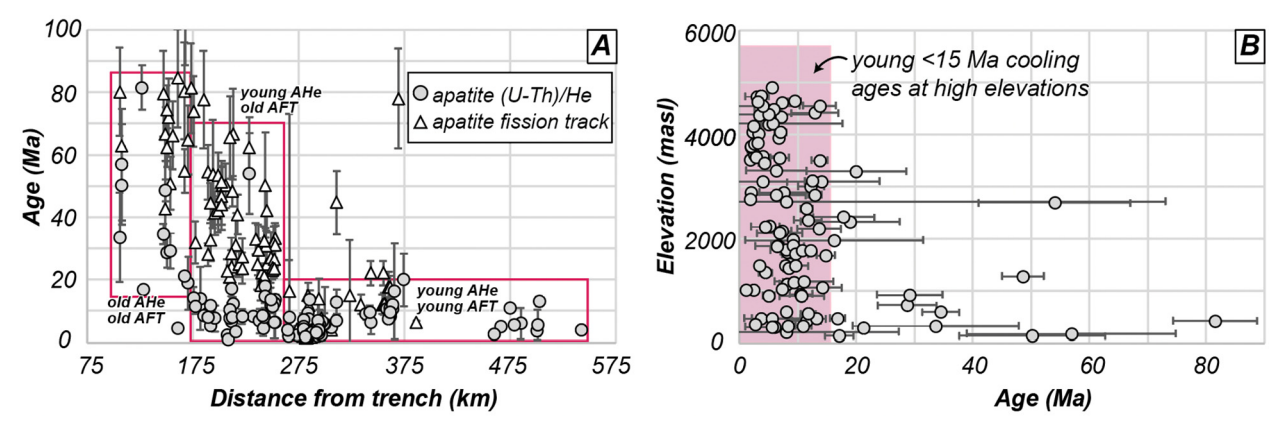


**Fig. 7.** (A) Cross-plot of distance from trench (km) versus cooling age (Ma) above the modern flat slab, north of the ridge axis. Note that the young cooling ages concentrate >175 km inboard from the trench. (B) Cross-plot of apatite (U-Th)/He age versus elevation for samples above the modern flat slab, north of the ridge axis (labeled distance from trench of 0 km in Fig. 5). Note the prevalence of young cooling ages at high elevation.

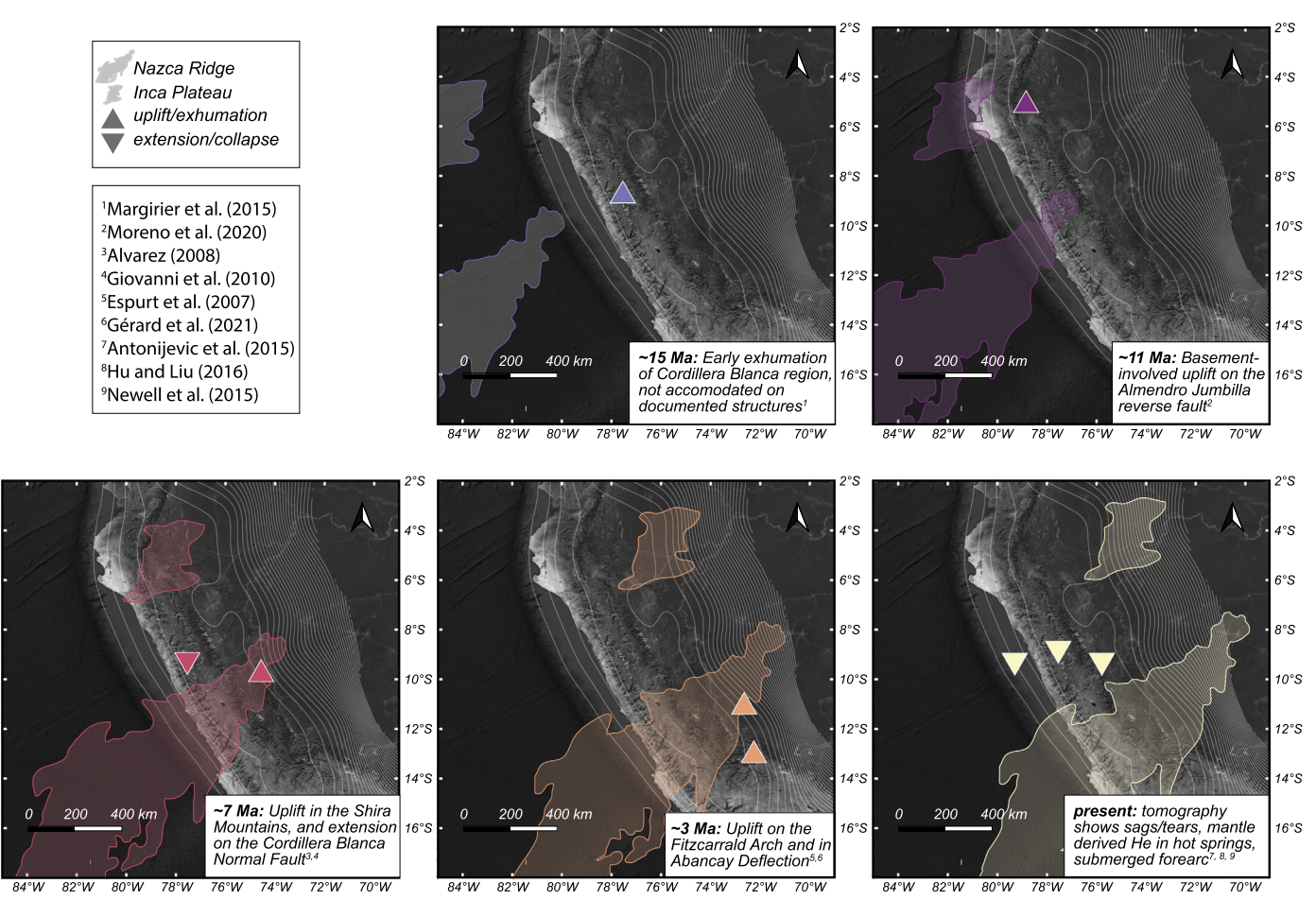


Fig. 8. Maps showing the location and timing of major geomorphic features in Peru that are explainable by uplift during aseismic ridge subduction and collapse after ridge passage. Location of ridge through time is from Rosenbaum et al. (2005). Benioff contours are shown at 20 km intervals.

Costa Rica (Morell, 2016), and are consistent with modeling that shows immediate uplift along the trench as the result of isostatic adjustments and thickening of the overriding plate upon ridge arrival (Espurt et al., 2008). A number of studies suggest that shallowing subduction leads to uplift in near-trench regions. For example, Gurnis (1992) demonstrated that shallow subduction induces isostatic uplift near the trench, with dynamic subsidence farther inboard. Near-trench uplift is detected in several studies of coastal and forearc areas along the Peruvian margin (von Huene and Suess, 1988; Hampel, 2002; Clift et al., 2003).

Here we review additional geologic evidence for the concentration of uplift and exhumation above the subducting ridge. A pulse of exhumation and uplift tracked the trajectory of the subducting ridge as it progressed from northern to southern Peru (Fig. 8). Sometimes the pulse of exhumation is accommodated on surface breaking structures, and in other cases it is not. Margirier et al. (2015) emphasized that the greater Cordillera Blanca region experienced early exhumation at  $\sim$ 15 Ma, roughly 10 Myr prior to initial detachment faulting (ca. 5.4 Ma; Giovanni et al., 2010). The lack of documented structures for this time period led the authors

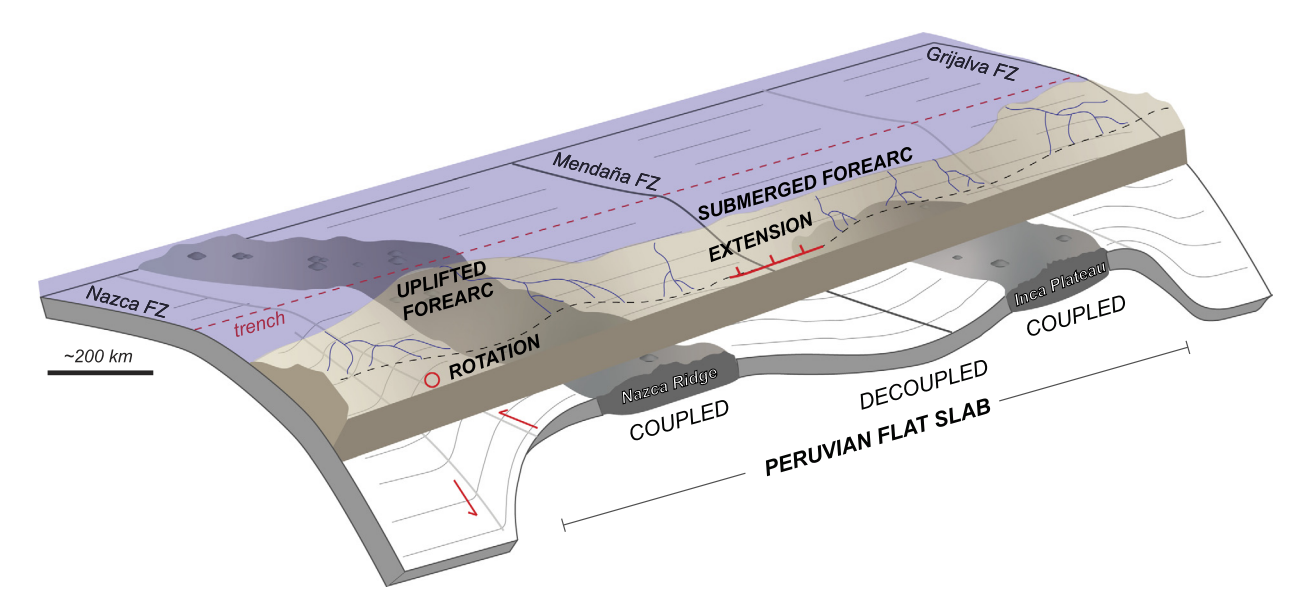


Fig. 9. Schematic diagram emphasizing the documented impacts of aseismic ridge subduction on the geomorphic evolution of the forearc and cordillera of the Peruvian margin. Geometry of the subducting plate is after Gutscher et al. (1999).

to suggest dynamic uplift associated with ridge arrival (Margirier et al., 2015). Uplift along the Eastern Cordillera in northmost Peru (5–6°S) commenced with the arrival of the Inca Plateau at the trench (ca. 13 Ma; Moreno et al., 2020). Here the Eastern Cordillera is brought up on a basement-involved high-angle structure, the Almendro Jumbilla Fault, though it likely shares a decollement with the rest of the fold-thrust belt. Moreno et al. (2020) suggest that uplift of the Eastern Cordillera at ca. 13 Ma, and that the Eastern Cordillera was acting as a drainage divide by ca. 11 Ma.

In the foreland, the Shira Mountains partitioned the surrounding basin between 7.2-5.3 Ma (Alvarez, 2008), coincident with the passage of the Nazca Ridge at these latitudes (9-11°S). Other features of potentially similar origins include the Cushabatay High, Contamana High, and Moa Divisor Range. The Fitzcarrald Arch (7.5–12.5°S) has been uplifting since ca. 4 Ma in the absence of surface breaking faults above the inboard projection of the Nazca Ridge (Espurt et al., 2007). Seismic tomographic data for the subducted segment of the Nazca Ridge indicate the removal of continental mantle lithosphere and displacement of lower crust forelandward (Bishop et al., 2018). It remains unclear whether bulldozing of lower crustal and continental mantle lithosphere occurs everywhere above the flat slab or is localized above the subducting ridge (Bishop et al., 2018). We suggest that the young cooling ages south of the current ridge location may reflect bulldozing of continental mantle lithosphere to lower crust in front of the southward-advancing ridge. The southward-migrating keel would induce rock uplift, which would generate increased erosion, and could explain the younger cooling ages in front of the ridge.

Exposure dating on terraces suggests coastal uplift above the modern trace of the Nazca Ridge (e.g., Hall et al., 2008; Saillard et al., 2011). Rosenbaum et al. (2005) also show a spatial and temporal coincidence between arrival of the Nazca Ridge at the trench and increased metallogenic activity. Such as immediate response in magmatism could represent a change in overriding plate stress that facilitates mobilization of fertile melts to shallow depths, promoting metal concentration in fractures.

Finally, Gérard et al. (2021) emphasize the Abancay Deflection within the Peruvian fold-thrust belt as a tectonic syntaxis with rapid incision and localized deformation since  $\sim$ 5 Ma. We suggest that the Abancay Deflection is the surface expression of the transition in the subducting slab from a steep to shallow configuration. Recent studies have suggested that subducting indenters

may promote syntaxial growth (Bendick and Ehlers, 2014). In such a scenario, coupling between the subducting and overriding plates above the subducting Nazca Ridge may be hindering subduction, leading to shear stresses along the transition to a normally dipping slab. We posit that these shear stresses lead to permanent strain in the overriding plate and are reflected in the rotation in the Abancay Deflection, and older rotational events farther north (Rousse et al., 2003).

# 5.2. Landscape relaxation in the wake of ridge passage

The thermochronometric and geomorphic data also imply that enhanced exhumation is not maintained across the entire zone of flat slab subduction. Instead, after the aseismic ridge propagates past a given area, the shallow slab no longer maintains the same degree of coupling between the subducting plate and the overriding plate (Fig. 9). If coupling were uniform across the entire  $\sim$ 1300 km along-strike extent of the flat slab, then all drainages would exhibit elevated catchment-averaged ksn and elevated erosion rates in all drainages above the entire flat slab region. Instead, erosion rates and channel steepness in west-draining catchments display the most elevated values proximal to the subducting Nazca Ridge and diminish to the north. Apatite (U-Th)/He ages provide chronologic constraints on upper-crustal cooling and suggest that exhumation commenced and terminated earlier in the north than in the south, with the peak cooling ages tracking progressive aseismic ridge subduction (Fig. 6).

Subsidence and collapse in the wake of ridge passage is also supported by regional geologic constraints. Normal faulting initiated at ca. 5.4 Ma in the Cordillera Blanca and has been used to argue for gravitational collapse following ridge passage (Giovanni et al., 2010). Nearby purported metamorphic core complex development also suggests large-scale crustal redistribution following ridge passage (McNulty and Farber, 2002). Hot springs near the Cordillera Blanca yield <sup>4</sup>He/<sup>3</sup>He ratios that suggest the presence of up to 25% mantle-derived helium, indicating either an asthenospheric source or mobilization from continental mantle lithosphere due to interactions with metasomatic fluids (Newell et al., 2015). Additionally, seismic, tomographic, and modeling studies indicate slab sags and minor tears between the Nazca Ridge and Inca Plateau, leading some to suggest mechanical failure of flat slab segments shortly after the passage of a buoyant feature (Fig. 1;

Gutscher et al., 1999; Antonijevic et al., 2015; Hu and Liu, 2016; Wagner and Okal, 2019). In many ways, extension in the wake of the ridge during slab sagging resembles processes observed during slab rollback and foundering. Extension in the wake of the ridge was likely preceded by significant crustal thickening (Coldwell et al., 2011), perhaps facilitated by lower crustal displacement. Once unsupported by physical coupling with the ridge, the thickened crust became gravitationally unstable, and underwent extensional collapse (sensu Dewey, 1988). These observations are critical for evaluating ancient flat slab systems, as mechanical coupling is likely restricted spatially and not maintained uniformly across the entire zone of arc shutoff and slab flattening.

# 6. Conclusions

Understanding how flat slab subduction and aseismic ridge subduction manifest in the rock record is critical for tracking orogenic evolution of Cordilleran margins. Subduction of the Inca Plateau and the Nazca Ridge under the Peruvian margin helped facilitate a flat slab geometry initiating around 10 Ma in northern Peru, which was towed southward behind the subducting Nazca Ridge, progressively shutting of magmatism in a southward sweep. Concentrated rock uplift and exhumation propagated southward with migration of the subducting Nazca Ridge. The uptick in exhumation is expressed by young cooling ages of low temperature thermochronometers, requiring  $\sim$ 2–3 kms of exhumation spatially restricted to regions the ridge passed ( $\sim$ 5-14°S). In the west, exhumation is not accommodated on surface breaking structures, but instead appears to be supported by ridge buoyancy. In the Eastern Cordillera and Subandean Zone, a combination of exhumation along discrete structures (e.g., Shira Mountains, Almendro Jumbilla Fault) and ridge buoyancy (e.g., Fitzcarrald Arch) seem to accommodate exhumation.

Though Peru has experienced protracted upper-plate deformation since the Late Cretaceous, a concentrated pulse of exhumation coincided with the trajectory and timing of the subducting ridge. In the case of the Peruvian flat slab, it seems that little coupling between the overriding and subducting plate persists after the Nazca Ridge propagates past. In broad paleo-flat slabs, large zones of arc shutoff are often spatially discrete from limited zones of exhumation. Our observations in Peru offer a mechanism to explain such patterns, where flat slab subduction drives broad arc shutoff, and exhumation is concentrated above subducting ridges.

# CRediT authorship contribution statement

**Sarah W.M. George:** Conceptualization, Methodology, Visualization, Writing – original draft. **Nicholas D. Perez:** Writing – review & editing. **William Struble:** Formal analysis, Methodology, Writing – review & editing. **Magdalena Ellis Curry:** Writing – review & editing. **Brian K. Horton:** Writing – review & editing.

# **Declaration of competing interest**

The authors declare that they have no known competing financial interests or personal relationships that could have appeared to influence the work reported in this paper.

# Data availability

Data is available in the Supplemental Materials.

# Acknowledgements

We thank Paul Kapp, Kurt Sundell, Audrey Margirier, Gilby Jepson, Federico Moreno, Chelsea Mackaman-Lofland, Tyler Grambling, Claire Currie, and Xiaowen Liu for discussions on flat slab processes, the Cordillera Blanca, and the thermal state of the lithosphere during flat slab subduction. Research was supported in part by an NSF grant (1847392) to NDP. Reviews and editorial support from Jiashun Hu, an anonymous reviewer, and Rebecca Bendick improved this manuscript.

#### Appendix A. Supplementary material

Supplementary material related to this article can be found online at https://doi.org/10.1016/j.epsl.2022.117754.

#### References

- Alvarez, J.O.S., 2008. Structural and Stratigraphic Evolution of Shira Mountains, Central Ucayali Basin, Perú. Doctoral dissertation. Texas A&M University.
- Antonijevic, S.K., Wagner, L.S., Kumar, A., Beck, S.L., Long, M.D., Zandt, G., Tavera, H., Condori, C., 2015. The role of ridges in the formation and longevity of flat slabs. Nature 524, 212–215.
- Barazangi, M., Isacks, B.L., 1976. Spatial distribution of earthquakes and subduction of the Nazca plate beneath South America. Geology 4 (11), 686–692. https://doi.org/10.1130/0091-7613(1976)4<686:sdoeas>2.0.co;2.
- Bendick, R., Ehlers, T.A., 2014. Extreme localized exhumation at syntaxes initiated by subduction geometry. Geophys. Res. Lett. 41 (16), 5861–5867.
- Bishop, B.T., Beck, S.L., Zandt, G., Wagner, L., Long, M., Antonijevic, S.K., Kumar, A., Tavera, H., 2017. Causes and consequences of flat slab subduction in southern Peru. Geosphere 13 (5), 1392–1407. https://doi.org/10.1130/GES01440.1.
- Bishop, B.T., Beck, S.L., George, Z., Wagner, L.S., Long, M.D., Tavera, H., 2018. Foreland uplift during flat subduction: insights from the Peruvian Andes and Fitzcarrald Arch. Tectonophysics 731–732, 73–84.
- Clift, P.D., Pecher, I., Kukowski, N., Hampel, A., 2003. Tectonic erosion of the Peruvian forearc, Lima Basin, by subduction and Nazca Ridge collision. Tectonics 22, 1023. https://doi.org/10.1029/2002TC001386.
- Codilean, A.T., Munack, H., Cohen, T.J., Saktura, W.M., Gray, A., Mudd, S.M., 2018. OCTOPUS: an open cosmogenic isotope and luminescence database. Earth Syst. Sci. Data 10, 2123–2139. https://doi.org/10.5194/essd-10-2123-2018.
- Coldwell, B., Clemens, J., Peford, N., 2011. Deep crustal melting in the Peruvian Andes: felsic magma generation during delamination and uplift. Lithos 125, 272–286.
- Dewey, J.F., 1988. Extensional collapse of orogens. Tectonics 7 (6), 1123-1139.
- Dickinson, W.R., Snyder, W.S., 1978. Plate Tectonics of the Laramide Orogeny, vol. 151. Geological Society of America, pp. 355–366.
- Eakin, C.M., Lithgow-Bertelloni, C., Davila, F.M., 2014. Influence of Peruvian flatsubduction dynamics on the evolution of western Amazonia. Earth Planet. Sci. Lett. 404, 250–260.
- Ehlers, T.A., Farley, K.A., 2003. Apatite (U-Th)/He thermochronometry: methods and applications to problems in tectonic and surface processes. Earth Planet. Sci. Lett. 206, 1–14.
- Espurt, N., Baby, P., Brusset, S., Roddaz, M., Hermoza, W., Regard, V., Antoine, P.O., Salas-Gismondi, R., Bolanos, R., 2007. How does the Nazca Ridge subduction influence the modern Amazonian foreland basin? Geology 35, 515–518.
- Espurt, N., Funiciello, F., Martinod, J., Guillaume, B., Regard, V., Faccenna, C., Brusset, S., 2008. Flat subduction dynamics and deformation of the South American plate: insights from analog modeling. Tectonics 27, TC3011. https://doi.org/10.1029/2007TC002175.
- Finzel, E.S., Trop, J.M., Ridgway, K.D., Enkelmann, E., 2011. Upper plate proxies for flat-slab subduction processes in southern Alaska. Earth Planet. Sci. Lett. 303 (3–4), 348–360. https://doi.org/10.1016/j.epsl.2011.01.014.
- George, S.W.M., Horton, B.K., Jackson, L., Moreno, F., Carlotto, V., Garzione, C.N., 2019. Sediment provenance variations during contrasting Mesozoic-early Cenozoic tectonic regimes of the northern Peruvian Andes and Santiago-Marañon foreland basin. In: Horton, B., Folguera, A. (Eds.), Andean Tectonics. 1. Elsevier, pp. 269–296.
- Gérard, B., Robert, X., Audin, L., Valla, P.G., Bernet, M., Gautheron, C., 2021. Differential exhumation of the Eastern Cordillera in the Central Andes: evidence for south-verging backthrusting (Abancay Deflection, Peru). Tectonics 40, e2020TC006314. https://doi.org/10.1029/2020TC006314.
- Giovanni, M.K., Horton, B.K., Garzione, C.N., McNulty, B., Grove, M., 2010. Extensional basin evolution in the Cordillera Blanca, Peru: stratigraphic and isotopic records of detachment faulting and orogenic collapse in the Andean hinterland. Tectonics 29, TC6007. https://doi.org/10.1029/2010TC002666.
- Gurnis, M., 1992. Rapid continental subsidence following the initiation and evolution of subduction. Nature.
- Gutscher, M.A., Maury, R., Eissen, J.P., Bourdon, E., 2000a. Can slab melting be caused by flat subduction? Geology 28 (6), 535–538.
- Gutscher, M.A., Spakman, W., Bijwaard, H., Engdahl, E.R., 2000b. Geodynamics of flat subduction: seismicity and tomographic constraints from the Andean margin. Tectonics 19, 814–833.

- Gutscher, M.A., Olivet, J.L., Aslanian, D., Eissen, J.P., Maury, R., 1999. The "lost inca plateau": cause of flat subduction beneath Peru? Earth Planet. Sci. Lett. 171 (3), 335–341.
- Hall, S.R., Farber, D.L., Audin, L., Finkel, R.C., Mériaux, A.S., 2008. Geochronology of pediment surfaces in southern Peru: implications for Quaternary deformation of the Andean forearc. Tectonophysics 459, 186–205.
- Hampel, A., 2002. The migration history of the Nazca Ridge along the Peruvian active margin: a re-evaluation. Earth Planet. Sci. Lett. 203, 665–679.
- Hampel, A., Kukowski, N., Bialas, J., Huebscher, C., Heinbockel, R., 2004. Ridge subduction at an erosive margin: the collision zone of the Nazca Ridge in southern Peru. J. Geophys. Res. 109, B02101. https://doi.org/10.1029/2003JB002593.
- Hayes, G.P., Moore, G.L., Portner, D.E., Hearne, M., Flamme, H., Furtney, M., Smoczyk, G.M., 2018. Slab2, a comprehensive subduction zone geometry model. Science 362 (6410), 58–61.
- Horton, B.K., 2018. Tectonic regimes of the central and southern Andes: responses to variations in plate coupling during subduction. Tectonics 37. https://doi.org/ 10.1002/2017TC004624.
- Hu, J., Liu, L., 2016. Abnormal seismological and magmatic processes controlled by the tearing South American flat slabs. Earth Planet. Sci. Lett. 450, 40–51.
- Jordan, T.E., Isacks, B.L., Allmendinger, R.W., Brewer, J.A., Ramos, V.A., Ando, C.J., 1983. Andean tectonics related to geometry of subducted Nazca plate. Geol. Soc. Am. Bull. 94 (3), 341–361. https://doi.org/10.1130/0016-7606(1983)94<341:
- Ketcham, R.A., Carter, A., Donelick, R.A., Barbarand, J., Hurford, A.J., 2007. Improved modeling of fission-track annealing in apatite. Am. Mineral. 92 (5–6), 799–810. https://doi.org/10.2138/am.2007.2281.
- Kirby, E., Whipple, K.X., 2012. Expression of active tectonics in erosional landscapes. J. Struct. Geol. 44, 54–75.
- Maloney, K.T., Clarke, G.L., Klepeis, K.A., Quevedo, L., 2013. The Late Jurassic to present evolution of the Andean margin: drivers and the geological record. Tectonics 32, 1049–1065. https://doi.org/10.1002/tect.20067.
- Manea, V.C., Manea, M., Ferrari, L., Orozco-Esquivel, T., Valenzuela, R.W., Husker, A., Kostoglodov, V., 2017. A review of the geodynamic evolution of flat slab subduction in Mexico, Peru, and Chile. Tectonophysics 695, 27–52.
- Margirier, A., Robert, X., Audin, L., Gautheron, C., Bernet, M., Hall, S., Simon-Labric, T., 2015. Slab flattening, magmatism and surface uplift in the Cordillera Occidental (northern Peru). Geology 43 (11), 1031–1034. https://doi.org/10.1130/G37061.1.
- Margirier, A., Audin, L., Robert, X., Herman, F., Ganne, J., Schwartz, S., 2016. Time and mode of exhumation of the Cordillera Blanca batholith (Peruvian Andes). J. Geophys. Res., Solid Earth 121, 6235–6249. https://doi.org/10.1002/2016JB013055.
- McNulty, B.A., Farber, D.L., 2002. Active detachment faulting above the Peruvian flat slab. Geology 30, 567–570.
- Mégard, F., 1984. The Andean orogenic period and its major structures in central and northern Peru. J. Geol. Soc. (Lond.) 141, 893–900.
- Morell, K.D., 2016. Seamount, ridge, and transform subduction in southern Central America. Tectonics 35, 357–385. https://doi.org/10.1002/2015TC003950.
- Moreno, F., Garzione, C.N., George, S.W.M., Horton, B.K., Williams, L., Jackson, L.J., Carlotto, V., Richter, F., Bandeian, A., 2020. Coupled Andean growth and foreland

- basin evolution, Campanian–Cenozoic Bagua Basin, northern Peru. Tectonics 39, e2019TC005967. https://doi.org/10.1029/2019TC005967.
- Newell, D.L., Jessup, M.J., Hilton, D.R., Shaw, C.A., Hughes, C.A., 2015. Mantle-derived helium in hot springs of the Cordillera Blanca, Peru: implications for mantle-to-curst fluid transfer in a flat-slab subduction setting. Chem. Geol. 417, 200–209.
- Pilger, R.H., 1981. Plate reconstructions, aseismic ridges, and low angle subduction beneath the Andes. Geol. Soc. Am. Bull. 92, 448–456.
- Ramos, V.A., Folguera, A., 2009. Andean flat slab subduction through time. Geol. Soc. (Lond.) Spec. Publ. (ISSN 0305-8719) 327 (1), 31–54. https://doi.org/10.1144/SP327.3.
- Rosenbaum, G., Giles, D., Saxon, M., Betts, P.G., Weinberg, R.F., Duboz, C., 2005. Subduction of the Nazca Ridge and the Inca Plateau: insights into the formation of ore deposits in Peru. Earth Planet. Sci. Lett. 239 (1–2), 18–32.
- Rosenbaum, G., Mo, W., 2011. Tectonic and magmatic responses to the subduction of high bathymetric relief. In: Island Arcs: Their Role in Growth of Accretionary Orogens and Mineral Endowment. Gondwana Res. 19 (3), 571–582. https://doi.org/10.1016/j.gr.2010.10.007.
- Rousse, S., Gilder, S., Farber, D., McNulty, B., Patriat, P., Torres, V., Sempere, T., 2003.

  Paleomagnetic tracking of mountain building in the Peruvian Andes since 10

  Ma. Tectonics 22 (5), 1048. https://doi.org/10.1029/2003TC001508.
- Saillard, M., Hall, S.R., Audin, L., Farber, D.L., Regard, V., Hrail, G., 2011. Andean coastal uplift and active tectonics in southern Peru: 10Be surface exposure dating of differentially uplifted marine terrace sequences (San Juan de Marcona, ~15.4S). Geomorphology 128, 178–190. https://doi.org/10.1016/j.geomorph.2011.01.004.
- Scherrenberg, A.F., Kohn, B.P., Holcombe, R.J., Rosenbaum, G., 2016. Thermotectonic history of the Marañón Fold–Thrust Belt, Peru: insights into mineralisation in an evolving orogen. Tectonophysics 667, 16–36. https://doi.org/10.1016/j.tecto. 2015.11.007.
- Schwanghart, W., Scherler, D., 2014. Short Communication: TopoToolbox 2 MATLAB-based software for topographic analysis and modeling in Earth surface sciences. Earth Surf. Dyn. 2, 1–7. https://doi.org/10.5194/esurf-2-1-2014.
- Spikings, R., Simpson, G., 2014. Rock uplift and exhumation of continental margins by the collision, accretion, and subduction of buoyant and topographically prominent oceanic crust. Tectonics 33, 635–655. https://doi.org/10.1002/2013TC003425
- Skinner, S.M., Clayton, R.W., 2013. The lack of correlation between flat slabs and bathymetric impactors in South America. Earth Planet. Sci. Lett.
- von Huene, R., Suess, E., 1988. Leg 112 shipboard scientific party, Ocean Drilling Program Leg 112, Peru continental margin: Part 1, tectonic history. Geology 16, 934–938. https://doi.org/10.1130/0091-7613(1988)016<0934:ODPLPC>2.3.CO;2.
- Wagner, L.S., Okal, E.A., 2019. The Pucallpa Nest and its constraints on the geometry of the Peruvian Flat Slab. Tectonophysics 762, 97–108.
- Wipf, M., Zeilinger, G., Seward, D., Schlunegger, F., 2008. Focused subaerial erosion during ridge subduction: impact on the geomorphology in south-central Peru. Terra Nova 20 (1), 1–10.